remote sensing

MDPI

Technical Note

Unmanned Aerial Vehicle-Based Hyperspectral Imaging Integrated with a Data Cleaning Strategy for Detection of Corn Canopy Biomass, Chlorophyll, and Nitrogen Contents at Plant Scale

Zhuolin Shi [1,2], Linglong Wang [1], Zengling Yang [1,2,*], Jinzhao Li [1], Linwei Cai [1], Yuanping Huang [1], Hongyan Zhang [2,3] and Lujia Han [1]

1 College of Engineering, China Agricultural University, Beijing 100083, China; shizhuolin@cau.edu.cn (Z.S.); wanglinglong@cau.edu.cn (L.W.); lijinzhao@cau.edu.cn (J.L.); cailw@cau.edu.cn (L.C.); hyping@cau.edu.cn (Y.H.); hanlj@cau.edu.cn (L.H.)
2 State Key Laboratory of Nutrient Use and Management, China Agricultural University, Beijing 100193, China; zhanghy@cau.edu.cn
3 College of Resources and Environmental Sciences, China Agricultural University, Beijing 100193, China
* Correspondence: yangzengling@cau.edu.cn; Tel.: +86-010-62736778

Abstract: The high-frequency detection of plant-scale crop growth in the field has great significance for achieving precise crop management and improving breeding practices. In this study, the biomass (BM), chlorophyll (Chl), and total nitrogen (TN) contents of the upper three leaves of the corn canopy are taken as examples, and unmanned aerial vehicle (UAV) and indoor hyperspectral imaging (HSI) detection models are established using partial least squares regression and support vector machine regression, respectively. The performance of the UAV HSI model was notably lower in comparison to the indoor model. Therefore, a UAV HSI data cleaning strategy integrated with RGB image information is further proposed, which involves eliminating data points with serious interference from information non-related to the plant. After data cleaning, the R^2_C of the BM, Chl, and TN contents detected through UAV HSI reached 0.537, 0.852, and 0.657, representing an improvement of over 70%. The $RMSE_P$ values were as low as 0.50 g, 2.2 SPAD, and 0.258%, which were comparable to those obtained with the indoor HSI detection model. This study demonstrates that UAV HSI integrated with the proposed data cleaning strategy can enable the rapid detection of corn canopy leaf properties at the plant scale in the field, supporting the high-frequency characterization of plant-scale crop growth parameters in the field.

Keywords: UAV; hyperspectral; crop growth; data cleaning; plant scale

Academic Editors: Xijian Fan, Yanjie Li, Sruti Das Choudhury, Shichao Jin and Cong (Vega) Xu

Received: 16 February 2025
Revised: 25 February 2025
Accepted: 28 February 2025
Published: 3 March 2025

Citation: Shi, Z.; Wang, L.; Yang, Z.; Li, J.; Cai, L.; Huang, Y.; Zhang, H.; Han, L. Unmanned Aerial Vehicle-Based Hyperspectral Imaging Integrated with a Data Cleaning Strategy for Detection of Corn Canopy Biomass, Chlorophyll, and Nitrogen Contents at Plant Scale. *Remote Sens.* **2025**, *17*, 895. https://doi.org/10.3390/rs17050895

1. Introduction

With increasingly extreme climates and growing food demand, precise crop management [1–4] and improved breeding practices [5–9] are crucial for achieving efficient food production with reduced inputs and environmental impact. This requires timely, convenient, and low-cost methods for the high-frequency characterization of crop growth at the plant scale [10,11].

Spectral technology has received increasing attention for the characterization of crop growth, due to its suitability for high-frequency analysis and its advantages of timeliness, convenience, and low cost. At present, indoor hyperspectral imaging (HSI) analysis is still the main method used for analyzing crop growth at the plant scale. For example, Ma [12] monitored the plant-scale biomass of corn plants using indoor HSI with nonlinear partial least squares analysis. Compared with indoor HSI, UAV HSI can directly enable the convenient and high-frequency analysis of crop growth in the field [13–15], which provides greater advantages. For example, Wang [16] monitored paddy rice nitrogen content and accumulation in plots with varying nitrogen treatment levels, while Liu [17] estimated potato above-ground biomass across field plots under different planting densities and fertilizer levels using UAV HSI. However, at present, most studies are still focused on the plot scale, and there are few studies focused on characterizing crops at the plant scale based on UAV HSI.

Compared with indoor HSI, UAV HSI still faces many challenges in accurately characterizing crop growth at the plant scale. Interference from information non-related to the plant, such as lodging, weeds, soil, adjacent plants, or miscellaneous items, is one such challenge. Data cleaning has been shown to be a feasible solution to solve the data interference problem in many studies [18]. Pereira [19] used a data cleaning method to solve the data offset interference problem caused by the inconsistent data acquisition methods used by different data collection teams. Hsiao [20] employed a data cleaning method to reduce the noise interference caused by random errors in high-resolution mass spectrometry and Raman spectroscopy data. Silalahi [21] used a data cleaning method to eliminate scattering interference in near-infrared spectroscopy data. Vašát [22] used a data cleaning method to eliminate the interference of non-sample signals in the visible–near-infrared spectroscopic detection of organic carbon in soil.

The canopy plays a crucial role in plant photosynthesis, where solar energy is captured and converted into chemical energy. Biomass (BM) directly reflects this process [23]. Chlorophyll (Chl), the key pigment in photosynthesis [24], also serves as an diagnostic tool for plant health [25]. Additionally, nitrogen content is an essential nutrient for plant growth [26]. Therefore, this study takes the BM, Chl, and total nitrogen (TN) contents of the upper three leaves of the corn canopy as the research objects to explore the feasibility of using UAV HSI to detect corn growth parameters at the plant scale in the field and the feasibility of using a data cleaning strategy to improve the detection performance. Also, the performance of the indoor model was used to verify the effect of the UAV HSI integrated with the data cleaning strategy on corn growth detection.

2. Materials and Methods

2.1. Study Site

The experiment was conducted in a long-term localization experimental field at the Quzhou Experimental Station of China Agricultural University (36°52′20.9″N, 115°01′20.0″E). The experiment was initiated in October 2007, and the wheat–corn double-crop rotation system was adopted, with wheat sown in early October and corn sown in mid-June. The wheat variety was Liangxing 99, and the corn variety was Zhengdan 958. The long-term localization experiment factors and level settings are detailed in Table 1, and the plot layout is shown in Figure 1.

Table 1. Long-term localization experiment factors and level settings.

Factor	Level	Abbreviations of the Treatments
Tillage method	Conservation tillage: corn is sown without tillage, while wheat is sown with tillage	CT
	No-tillage: wheat and corn are sown without tillage	NT

Table 1. *Cont.*

Factor	Level	Abbreviations of the Treatments
Stubble return	Wheat and corn straws are not returned to the fields within one year	C0
	Wheat straw is returned to the field, while the corn straw is not returned to the field within one year	C1
Nitrogen fertilizer application rate	Application rate per season: 120 kg hm^{-2}	N1
	Application rate per season: 180 kg hm^{-2}	N2
	Application rate per season: 240 kg hm^{-2}	N3

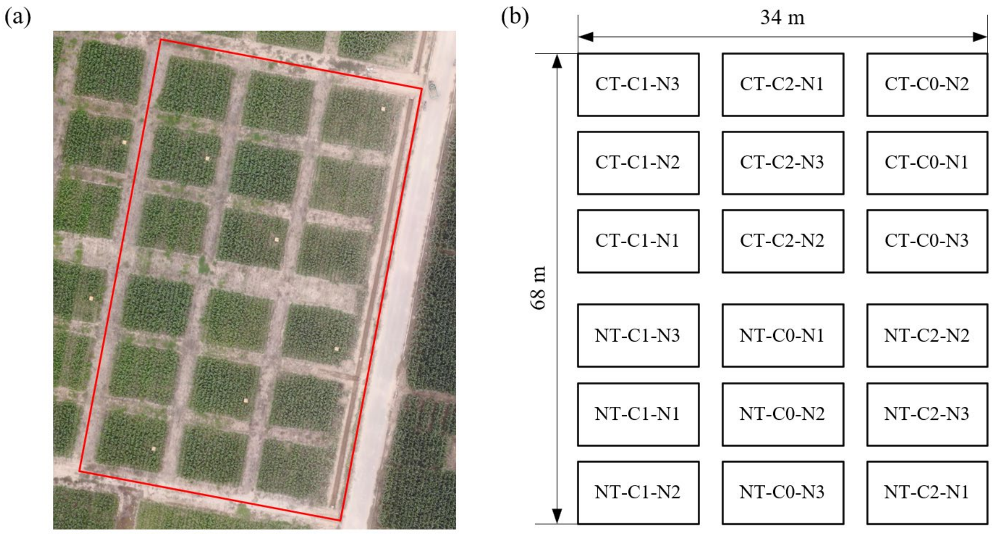

Figure 1. Long-term localization experiment plot map: (**a**) UAV aerial photo of the test plot, where the red box indicates the test plot; (**b**) schematic diagram of the test plot layout, where X in X-Y-Z represents the tillage method, Y represents the straw return treatment, and Z represents the nitrogen fertilizer application rate. The abbreviations of the treatments are provided in Table 1.

2.2. Field Measurements

In September 2023, UAV HSI data were first collected in the aforementioned field. Subsequently, 5 plants were randomly selected from each plot, amounting to a total of 90 corn plants across 18 plots, as research objects. During the sampling process, a Galaxy 1 RTK-GNSS measuring instrument (Southern Surveying and Mapping, Guangzhou, China) was used to record the longitude and latitude coordinates (with an error margin of 2 cm) of each corn plant.

2.3. Laboratory Measurements

Indoor HSI data were collected immediately after the collection of the corn samples, following which the upper 3 leaves on the corn plants were separated. The SPAD values were measured at 15 points across the upper 3 leaves of each corn plant using a SPAD-502 chlorophyll meter (Konica Minolta, Tokyo, Japan), and the average SPAD values were calculated to represent the Chl level. Subsequently, the samples were placed in an oven at 105 °C for 30 min and dried at 75 °C. When the weight of the sample no longer changed, the weight was recorded as the BM value. The samples were ground using a TissueLyser II ball mill (QIAGEN, Hilden, Germany) until they passed through a 20-mesh sieve. The TN content of the corn canopy leaves was determined using an elemental analyzer (Vario Macro, Elementar, Langenselbold, Germany). Two sets of parallel measurements were performed for each sample, and the average value was taken.

2.4. UAV Data Acquisition and Preprocessing

2.4.1. Data Acquisition of UAV HSI

On a clear and windless noon, a Matrice 300 RTK drone (DJI, Shenzhen, China) equipped with a hyperspectral camera (FIREFLEYE 185, Cubert, Ulm, Germany) was used to obtain HSI data of the corn canopy in the long-term localization experimental field. Figure 2a shows the UAV hyperspectral system. FIREFLEYE 185 captures 125 channels of HSI in the 450–950 nm range in real-time. The flight speed was 4 m/s. The heading and lateral overlap rates were set to 75% and 65%, respectively. The altitude was 35 m, with a ground sampling distance (GSD) of 1.41 cm/pixel. As shown in Figure 2b, a 300 × 300 mm 95% reflectance whiteboard (SphereOptics, Herrsching, Germany) was used to collect reference images before takeoff. The operator positioned the UAV facing the sun to fill the camera's field of view with the reference board, avoiding shadows. The lens was covered to capture dark backgrounds. Data were exported to a workstation. Utils Touch software (Cubert, Ulm, Germany) corrected hyperspectral photos to reflectance photos. Matching panchromatic images were exported for image mosaicking.

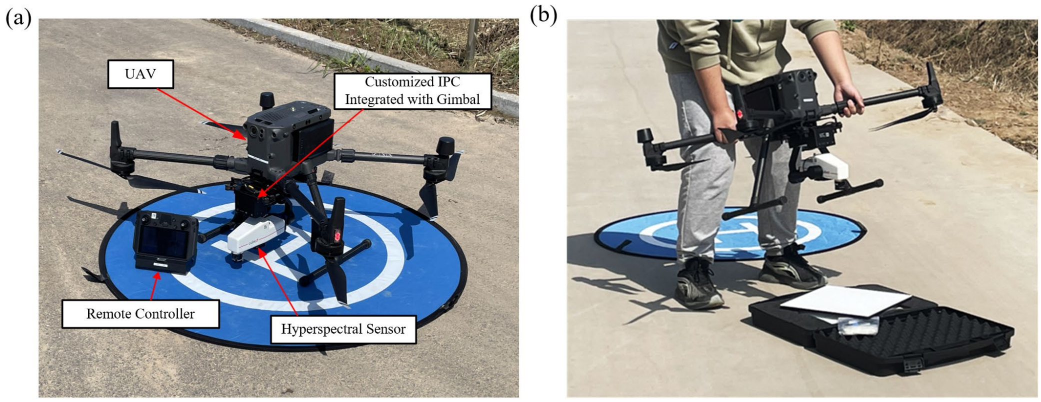

Figure 2. UAV hyperspectral system: (**a**) system composition; (**b**) reference acquisition.

2.4.2. Data Acquisition of UAV RGB Imaging

A Mavic3M drone (DJI, Shenzhen, China) equipped with an RGB camera was utilized to capture the RGB data of the experimental field at the institute. During data collection, the flight speed was 8 m/s; the heading overlap rate and the side overlap rate were set to 75% and 65%, respectively; the flight altitude was set to 50 m; and the ground sampling distance (GSD) was 1.375 cm/pixel.

2.4.3. Coordinate Alignments and UAV Image Mosaicking

In order to accurately locate the plant-scale corn research objects in the UAV imagery, ground control points (GCPs) were arranged around and in the center of the experimental field. As shown in Figure 3, the placement of the GCPs in the field was realized using a hollow steel pipe inserted into the ground and a position marker plate inserted into the ground, and GCPs on the asphalt road were realized by painting. All GCPs were recorded with the longitude and latitude coordinates of the CGCS2000 coordinate system using the RTK-GNSS measuring instrument.

UAV HSI and RGB data were stitched using Agisoft Metashape Professional (Agisoft LLC, St. Petersburg, Russia) with the Structure from Motion (SFM) algorithm, involving the following steps:

1. UAV image data were imported, the images were aligned according to the matching points in the overlapping area of the images, and a sparse point cloud was generated;

2. The locations of the GCPs in the image data were marked and inserted into the coordinates recorded by Galaxy 1 in order to optimize the alignment results;
3. A dense point cloud was generated, and a 3D mesh model was constructed;
4. An orthophoto with accurate position information was generated and exported.

Figure 3. Arrangement of GCP and recording of coordinate information.

To save computing power, the operations on the UAV HSI data before generating orthophotos were accomplished using panchromatic images. When generating orthophotos, the hyperspectral reflectance image corresponding to the spatial pixels was utilized and exported as a UAV hyperspectral reflectance orthophoto.

Some representations of the UAV HSI and RGB orthophoto for corn canopy are shown in Figure 4. The UAV RGB orthophoto has richer texture information than the UAV HSI orthophoto, so the UAV RGB orthophoto was employed for subsequent data cleaning.

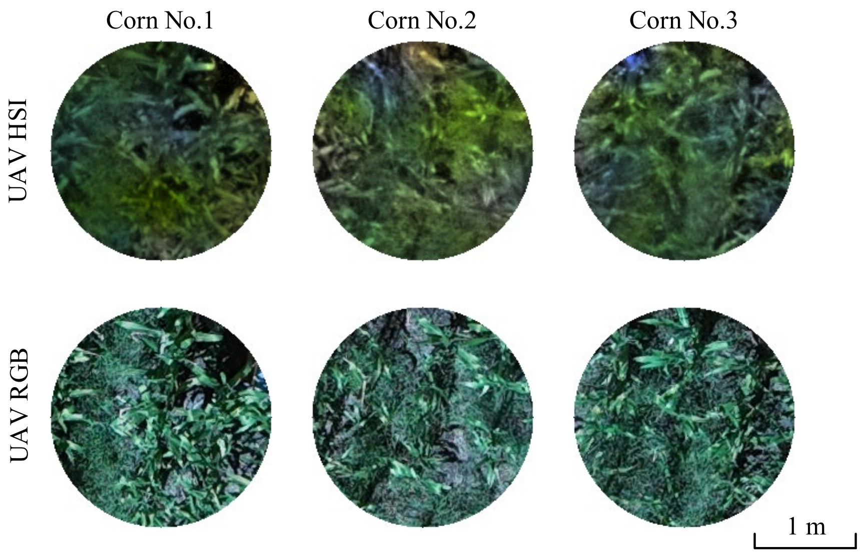

Figure 4. Representative UAV HSI and RGB orthophoto for corn canopy.

2.4.4. Spectral Extraction

The UAV hyperspectral reflectance orthophoto and the location coordinates of all the samples of the studied corn plants were imported into ArcGIS (Esri, Redlands, CA, USA). A circle with a diameter of 1 m was drawn with the coordinates as the center in order to define the Region of Interest (ROI), and the average reflectance within an ROI was calculated as the UAV reflectance spectrum of the corn canopy leaves at the plant scale.

2.5. Indoor Data Acquisition and Preprocessing

2.5.1. Data Acquisition of Indoor HSI

A visible–near-infrared hyperspectral camera with a wavelength range of 400–1000 nm (Image-λ-V10E, Dualix, Wuxi, China) was utilized to capture the hyperspectral data of each corn canopy leaf in the darkroom. A custom HSI measurement station, as shown in Figure 5, was used to scan the sample. This station used a horizontal motor to move the hyperspectral camera in the horizontal direction, thereby enabling spectral imaging data acquisition of corn canopy leaves at the plant scale. The vertical motor was utilized to control the camera's vertical movement, ensuring a fixed object distance of 70 cm in this study. Six 50 W DC halogen lamps, positioned with fixed relative locations to the camera, served as light sources. The scanning parameters of the camera were as follows: The Image-λ-V10E facet array sensor can simultaneously capture 960 × 176 pixel data in both spatial and spectral dimensions and is equipped with an HSIA-OLE23 imaging lens. It is configured with an exposure time of 23 ms, a frame rate of 43 Hz, and a scanning speed of 1.15 cm/s. Precise focusing was achieved by manually fine-tuning the camera's lens focusing ring. A 300 × 300 mm whiteboard (SphereOptics, Herrsching, Germany) with 95% reflectivity was used as a reflectance correction material. The camera dark current signal was collected every 30 min. During the scanning process, the indoor environment was maintained under stable conditions with minimized ambient light interference.

Figure 5. Schematic diagram of darkroom HSI measurement station.

2.5.2. Reflectance Correction

The hyperspectral raw data of plant-scale corn canopy leaves were corrected to reflectance data using scanning whiteboard data and dark current signal data. Whiteboard signals and dark current signals from the corresponding pixels of the sensor were employed for the correction of each data point.

The reflectance calculation formula is as follows:

$$R_{ijk} = \frac{D_{ijk} - B_{jk}}{W_{jk} - B_{jk}} \Big/ Ref, \tag{1}$$

where R_{ijk} is the reflectance of the kth band of the pixel in Row i and Column j of the hyperspectral raw data; D_{ijk} is the original digital signal value of the kth band of the pixel in Row i and Column j; W_{jk} is the original digital signal value of the kth band of the pixels in Column j of the scanned whiteboard; B_{jk} is the original digital signal value of the kth band of the pixels in Column j of the dark current data; and Ref is the reflectance of the whiteboard, which is 95% in this study.

2.5.3. ROI Marking and Spectral Extraction

The extraction of plant-scale corn canopy leaf spectra from the hyperspectral reflectance data cube of plant-scale corn canopy leaves involved the following steps:

1. The reflectances in the near-infrared (814 nm) and red (674 nm) bands were used to calculate the ratio vegetation index (RVI), and pixels with an RVI ratio exceeding 2 were marked as the mask area.
2. The pixels marked as vegetation in the mask were connected to form contiguous regions. Any regions with an area of less than 100 pixels were excluded from the mask. This process ensures that all masks correctly delineate the corn canopy leaf area, as shown in Figure 6.
3. The average spectrum corresponding to the mask area was extracted and calculated from the hyperspectral reflectance data cube of corn canopy leaves at the plant scale, that is, the corn canopy leaf spectrum of the corresponding sample.

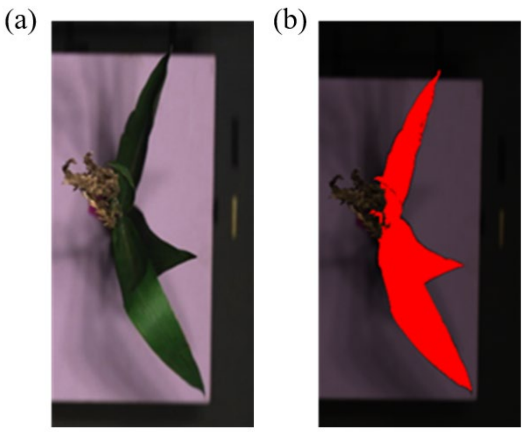

Figure 6. Schematic diagram of the ROI mask for corn canopy leaves: (**a**) pseudo-color image of hyperspectral reflectance; (**b**) pseudo-color image of the hyperspectral reflectance of the marked mask area.

2.6. Model Development and Evaluation

The whole dataset was divided into a calibration set and an external independent validation set in a ratio of 3:1 according to the BM, Chl, or TN content gradients. To ensure the applicability of the calibration model, the samples with the highest and lowest BM, Chl, or TN contents were included in the calibration set. Autoscaling was applied to standardize the variables in the spectrum before model development. Subsequently, two typical machine learning methods were employed to establish quantitative models for the BM, Chl, and TN contents in corn canopy leaves at the plant scale. These methods included partial least squares regression (PLSR) for linear modeling and support vector machine regression (SVMR) for nonlinear modeling.

Model evaluation indicators included the coefficient of determination (R^2_C for calibration, R^2_P for validation) and root mean square error ($RMSE_C$ for calibration, $RMSE_P$ for validation). Higher R^2_C and lower $RMSE_C$ show good calibration, while higher R^2_P and lower $RMSE_P$ indicate strong prediction performance. Similar $RMSE_C$ and $RMSE_P$ values suggest not overfitting.

2.7. Data Cleaning of UAV HSI Data Based on RGB Information

To mitigate the impact of abnormalities such as lodging, weeds, soil, adjacent plants, or miscellaneous items (Figure 7) on plant-scale crop growth monitoring using UAV HSI, this study identified outlier samples by analyzing texture information from RGB orthophoto images corresponding to target corn plant locations. HSI data points associated with outlier plant samples were marked as invalid.

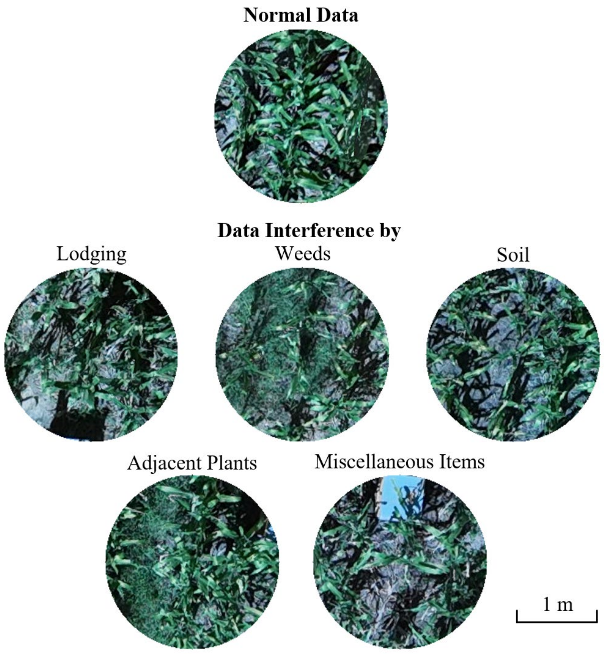

Figure 7. Examples of normal data and data interference by different factors.

Gray Level Co-occurrence Matrix (GLCM) [27] is a popular algorithm for texture feature extraction from images. Previous research [28] has shown that 4 typical textural features—contrast (CON), correlation (COR), energy (EN), and homogeneity (HO)—are useful for UAV-based crop growth monitoring. CON represents the local intensity contrast and texture coarseness, which may reflect the abnormalities caused by weeds or soil. COR measures the linear relationship between neighboring pixels and reflects the degree of similarity in texture patterns, which may reflect varying abnormalities. EN represents the sum of the squared elements in the GLCM, representing the overall texture energy or uniformity, which may reflect the abnormalities caused by adjacent plants. HO quantifies the closeness of the elements in the GLCM, reflecting the smoothness and homogeneity of the texture, which may also reflect the abnormalities caused by adjacent plants.

Therefore, 4 texture features—CON, COR, EN, and HO—were extracted from the red, green, and blue bands of RGB orthophoto images at corn plant sample locations using the GLCM. As RGB images contain 3 bands, each yielding 4 texture features, a total of 12 texture features were obtained for all targets. Outlier samples were identified based on whether their texture features exceeded twice the standard deviation, and any sample exhibiting outlier texture features across any band was flagged as invalid.

2.8. Software for Data Analysis

In the above data processing steps, image stitching was implemented in Metashape Professional, extraction of the UAV reflectance spectra of corn canopy leaves at the plant scale was carried out in ArcGIS, and the remaining steps were programmed in MATLAB 9.0 R2016a (MathWorks, Natick, MA, USA).

3. Results and Discussion

3.1. Analysis of Corn Canopy BM, Chl, and TN Contents and Hyperspectral Characteristics

The statistical analysis of the laboratory results is shown in Table 2. The range of BM was 0.79–5.16 g, the range of Chl was 30.4–57.7 SPAD, and the range of TN content was 1.681–4.095%. Analysis of the content distribution showed some variations (CV ranged from 0.11 to 0.39) in the properties of the tested samples, which is in line with the samples originating from the test plots using various tillage methods, straw return treatments, and nitrogen fertilizer application rates. The means and SDs for the whole set, calibration set, and validation set were similar, indicating that both the calibration set and the validation set have good representativeness.

Table 2. Statistical results of BM (biomass), Chl (chlorophyll), and TN (total nitrogen) contents in corn canopy leaf samples at the plant scale.

Property		*n*	Min	Max	Mean	SD	CV
BM (g)	Whole set:	90	0.79	5.16	2.06	0.79	0.38
	Calibration set:	67	0.79	5.16	2.05	0.79	0.39
	Validation set:	23	0.91	3.74	2.10	0.79	0.38
Chl (SPAD)	Whole set:	90	30.4	57.7	46.2	5.09	0.11
	Calibration set:	67	30.4	57.7	46.1	5.09	0.11
	Validation set:	23	36.4	57.0	46.6	5.18	0.11
TN (%)	Whole set:	90	1.681	4.095	2.720	0.472	0.174
	Calibration set:	67	1.681	4.095	2.705	0.466	0.172
	Validation set:	23	2.118	3.874	2.762	0.496	0.179

Abbreviations: Min—minimum, Max—maximum, SD—standard deviation, CV—coefficient of variation.

As the snapshot UAV HSI used in this study was obtained by bicubic interpolation sharpening, the plant-scale corn canopy leaf signals in the HSI contained interference from neighboring pixels. Therefore, in this study, RGB images were employed to identify and eliminate the data points with interference by corn lodging, weeds, soil, adjacent plants, or miscellaneous items in order to clean the UAV HSI data. A total of 22 sample points were removed, and a comparison of the BM, Chl, and TN content distributions in the sample set before and after data cleaning is shown in Figure 8. According to the data presented in the figure, there was no statistical difference ($p > 0.05$) between the calibration or validation set, and the distributions of the BM, Chl, and TN contents in the sample set after data cleaning presented no changes ($p > 0.05$), indicating that data cleaning did not affect the representativeness of the sample.

The reflectance spectrum curves of the plant-scale corn canopy leaves based on UAV and indoor HSI are presented in Figure 9. The overall law of the reflectance spectra was consistent between the two technologies. In particular, there is a red edge band with a sharp increase in reflectance at about 720 nm, and the reflectance is generally high in the near-infrared band, which was consistent with the literature report [29]. However, even for the same sample, differences in the reflectance spectra of the plant-scale corn canopy leaf based on UAV and indoor HSI were observed. Both groups of spectra had abnormally high reflectance at the beginning of the band, and the reflectance of the UAV HSI had an abnormal decrease after 890 nm, which was due to the lower quality of the spectral response of the edge pixels of the sensor [30]. The reflectance of the UAV HSI data in the near-infrared band was notably higher than that of the indoor HSI data, which was caused by the reflectance correction method and environmental factors [31]. The variability in the two sets of reflectance spectra was not significantly different ($p > 0.05$), indicating that both sets of spectral data successfully captured the spectral variation caused by differences between samples. The spectral mean and spectral variation in the samples after data cleaning did not change significantly ($p > 0.05$) when compared with those before data cleaning, indicating that data cleaning did not affect the representativeness of the spectra.

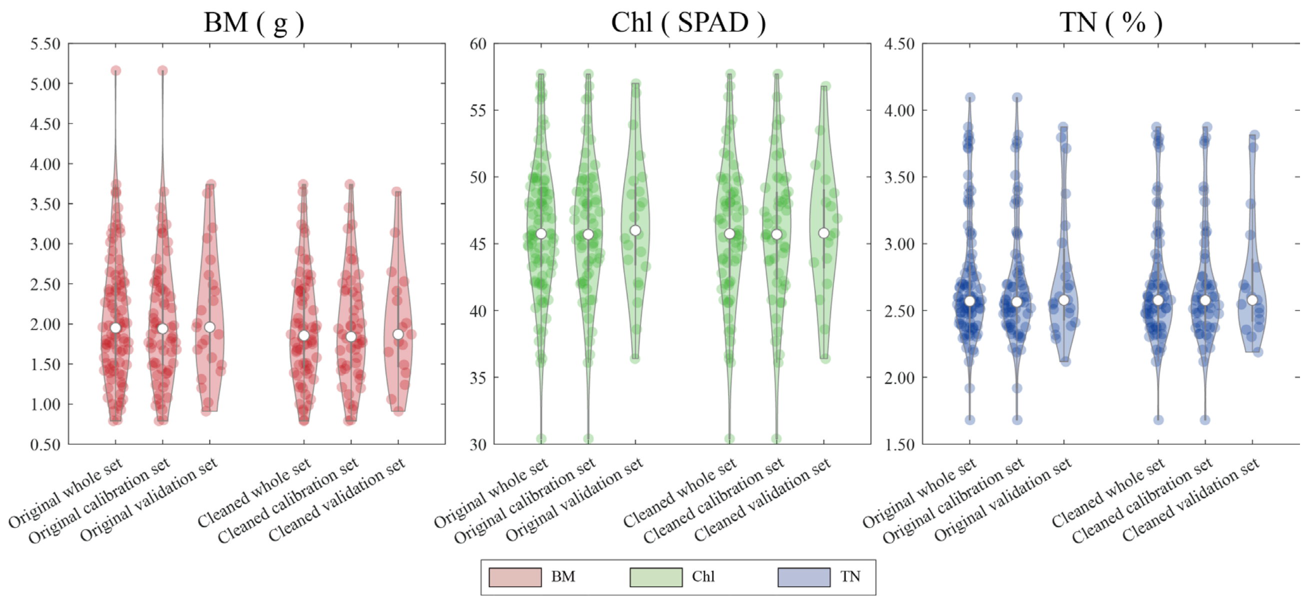

Figure 8. Violin plots of BM (biomass), Chl (chlorophyll), and TN (total nitrogen) content distributions in sample sets before and after data cleaning.

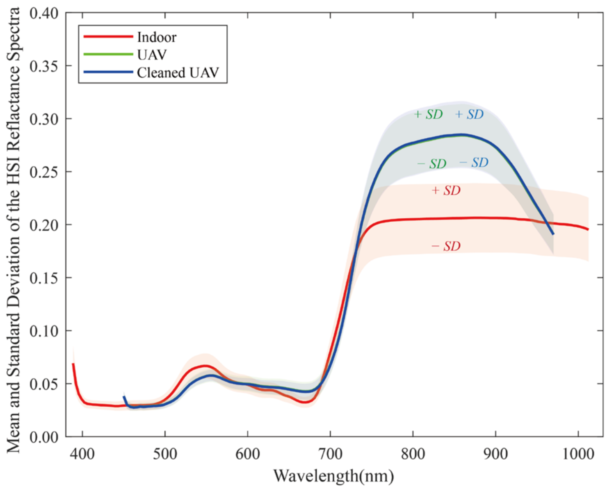

Figure 9. Spectral reflectance curve of corn canopy leaves at plant scale (UAV) and indoor HSI with mean values and standard deviation.

3.2. Detection Model for Plant-Scale Corn Canopy BM, Chl, and TN Contents

A linear method, PLSR, and a nonlinear method, SVMR, were employed to establish detection models for the BM, Chl, and TN contents based on UAV HSI and indoor HSI, respectively. The results of these models are shown in Figure 10. The R^2_C values of the detection models for the BM, Chl, and TN contents with the indoor HSI were 0.567, 0.899, and 0.702, respectively, and the $RMSE_P$ values were as low as 0.52 g, 1.9 SPAD, and 0.282%, respectively. In contrast, the R^2 values for the UAV HSI detection model were all below 0.5, and the $RMSE_P$ values were 0.69 g, 3.8 SPAD, and 0.385%, respectively, indicating a considerable disparity in performance when compared to the indoor HSI detection model.

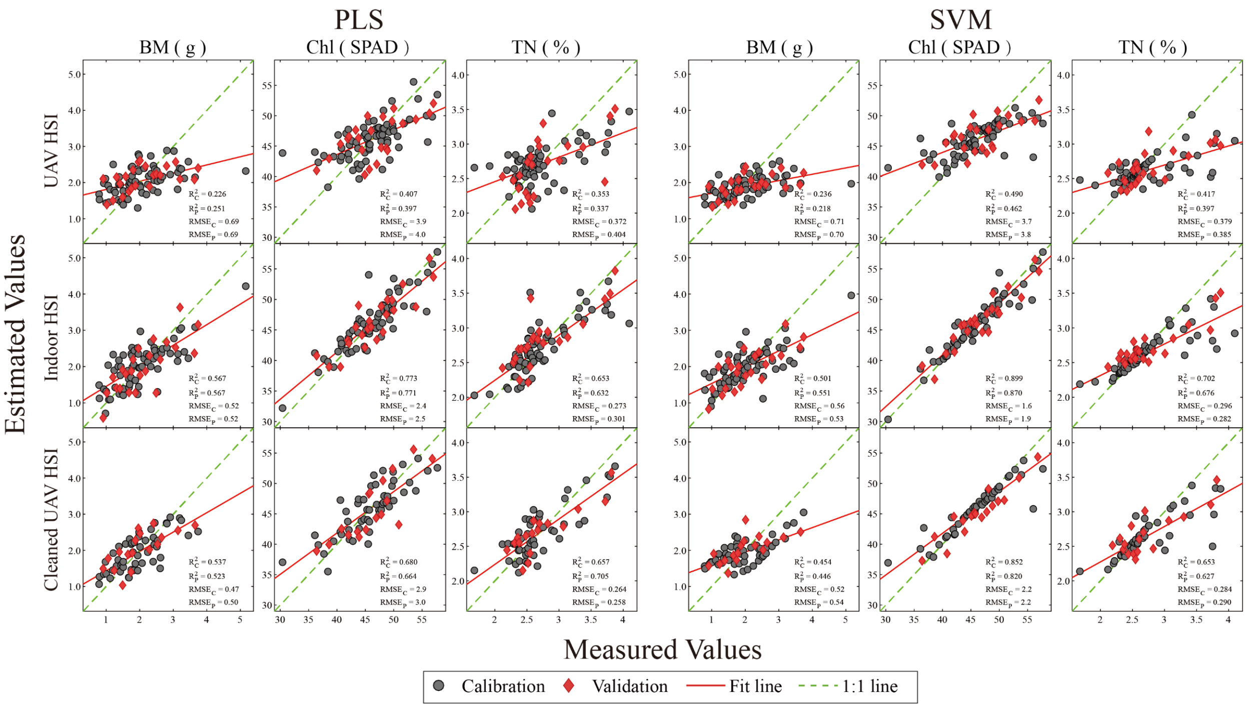

Figure 10. Evaluation of the plant-scale corn canopy leaf property detection models based on UAV HSI and indoor HSI before and after data cleaning.

3.3. Effect of Data Cleaning on Plant-Scale Corn Canopy BM, Chl, and TN Contents

After data cleaning, the $R^2{}_C$ values of the BM, Chl, and TN contents detected with the UAV HSI reached 0.537, 0.852, and 0.657, respectively, representing an improvement of over 70% when compared to that before data cleaning. The evaluation results on $RMSE_P$ were also impressive: BM was detected as low as 0.50 g, nearly matching the 0.52 g achieved by the indoor HSI detection model; Chl was detected as low as 2.2 SPAD, which showed greater precision than the 5.57 SPAD and 2.65 SPAD obtained with UAV HSI detection models in previous studies [32,33] and was similar to the 1.9 SPAD achieved by indoor HSI detection in this study; and TN was detected as low as 0.258%, which was superior to the 0.282% achieved by the indoor HSI detection model in this study and showed greater precision than the 0.521% and 0.26% obtained with UAV HSI detection models in previous studies [34,35] using SVMR.

The above results demonstrate that UAV HSI technology integrated with the data cleaning strategy is an effective method to enhance the performance of plant-scale corn canopy leaf property detection and is also a feasible solution for the rapid detection of plant-scale corn canopy leaf properties in the field. For this long-term localization experimental field, this study provides technical support for a more detailed high-frequency characterization of the effects of tillage, straw, and nitrogen management on corn growth within the wheat–corn rotation system.

3.4. Limitations and Future Work

This study presents a data cleaning strategy for plant-scale crop growth monitoring by UAV HSI. However, only four typical texture features extracted from GLCM are employed in this paper. Among them, EN and HO are too sensitive to abnormalities caused by adjacent plants, and there are many duplicates of anomalous samples identified by these two features (Figure S1). At the same time, this study only tested data from one collection task in one growth stage, but texture features are inevitably affected by crop growth stages and environmental conditions such as ambient light, which challenges the robustness of the present method.

There have been many texture feature extraction methods based on machine vision and deep learning available, and novel texture feature extraction methods can be explored in further research to improve the performance and robustness of abnormality identification.

Furthermore, this study only employed a cleaning method which involves eliminating interfering data points. Subsequent research can further accurately eliminate interfering data points in the pixel point set, thereby further enhancing the detection accuracy of plant-scale corn canopy leaf properties using UAV HSI.

4. Conclusions

This study proposed a strategy for UAV HSI data cleaning through the fusion of RGB image information, allowing for the removal of data points with serious interference from information non-related to the plant. After data cleaning, the R^2_C values of corn canopy leaf properties detected using UAV HSI represented an improvement of over 70%. The $RMSE_P$ values were as low as 0.50 g, 2.2 SPAD, and 0.258%, which were comparable to or even better than the 0.52 g, 1.9 SPAD, and 0.282% achieved with the indoor HSI detection model in this study. The results demonstrate that abnormalities such as lodging, weeds, soil, adjacent plants, or miscellaneous items interfere with plant-scale crop monitoring. However, this study only applied the data cleaning method of data removal based on texture features of UAV RGB images, which may not work well under varying growth stages or environmental conditions. In the future, more advanced data cleaning methods can be tried to reduce the interference of the aforementioned abnormalities. The results of this study demonstrate the feasibility of using UAV HSI integrated with the proposed data cleaning strategy to rapidly detect plant-scale corn canopy leaf properties in the field, providing technical support for the high-frequency characterization of plant-scale crop growth parameters in the field.

Supplementary Materials: The following supporting information can be downloaded at: https://www.mdpi.com/article/10.3390/rs17050895/s1, Figure S1. RGB orthophoto of anomalous samples identified by CON, COR, EN, and HO texture features from GLCM.

Author Contributions: Conceptualization, Z.S. and Z.Y.; methodology, Z.S.; software, Z.S.; validation, L.W., J.L. and Y.H.; formal analysis, L.W.; investigation, L.C. and Z.S.; resources, Z.Y. and H.Z.; data curation, Z.S.; writing—original draft preparation, Z.S.; writing—review and editing, Z.Y.; visualization, Z.S.; supervision, Z.Y.; project administration, L.H.; funding acquisition, Z.Y. All authors have read and agreed to the published version of the manuscript.

Funding: This research was funded by the National Key R&D Program of China (2022YFD2002101).

Data Availability Statement: The data presented in this study are available on request from the corresponding author.

Conflicts of Interest: The authors declare no conflicts of interest.

References

1. Godfray, H.C.J.; Garnett, T. Food Security and Sustainable Intensification. *Philos. Trans. R. Soc. B Biol. Sci.* **2014**, *369*, 20120273. [CrossRef] [PubMed]
2. Hedley, C. The Role of Precision Agriculture for Improved Nutrient Management on Farms: Precision Agriculture Managing Farm Nutrients. *J. Sci. Food Agric.* **2015**, *95*, 12–19. [CrossRef] [PubMed]
3. Sapkota, T.B.; Jat, M.L.; Rana, D.S.; Khatri-Chhetri, A.; Jat, H.S.; Bijarniya, D.; Sutaliya, J.M.; Kumar, M.; Singh, L.K.; Jat, R.K.; et al. Crop nutrient management using Nutrient Expert improves yield, increases farmers' income and reduces greenhouse gas emissions. *Sci. Rep.* **2021**, *11*, 1564. [CrossRef]
4. Wang, G.; Shi, R.; Mi, L.; Hu, J. Agricultural Eco-Efficiency: Challenges and Progress. *Sustainability* **2022**, *14*, 1051. [CrossRef]
5. Bailey-Serres, J.; Parker, J.E.; Ainsworth, E.A.; Oldroyd, G.E.D.; Schroeder, J.I. Genetic Strategies for Improving Crop Yields. *Nature* **2019**, *575*, 109–118. [CrossRef]

6. Varshney, R.K.; Bohra, A.; Roorkiwal, M.; Barmukh, R.; Cowling, W.A.; Chitikineni, A.; Lam, H.-M.; Hickey, L.T.; Croser, J.S.; Bayer, P.E.; et al. Fast-Forward Breeding for a Food-Secure World. *Trends Genet.* **2021**, *37*, 1124–1136. [CrossRef]
7. Huang, X.; Huang, S.; Han, B.; Li, J. The Integrated Genomics of Crop Domestication and Breeding. *Cell* **2022**, *185*, 2828–2839. [CrossRef]
8. Gu, Z.; Gong, J.; Zhu, Z.; Li, Z.; Feng, Q.; Wang, C.; Zhao, Y.; Zhan, Q.; Zhou, C.; Wang, A.; et al. Structure and Function of Rice Hybrid Genomes Reveal Genetic Basis and Optimal Performance of Heterosis. *Nat. Genet.* **2023**, *55*, 1745–1756. [CrossRef]
9. Aswini, M.S.; Kiran; Lenka, B.; Shaniware, Y.A.; Pandey, P.; Dash, A.P.; Haokip, S.W. The Role of Genetics and Plant Breeding for Crop Improvement: Current Progress and Future Prospects. *Int. J. Plant Soil Sci.* **2023**, *35*, 190–202. [CrossRef]
10. Bauer, J.; Aschenbruck, N. Towards a Low-Cost RSSI-Based Crop Monitoring. *ACM Trans. Internet Things* **2020**, *1*, 1–26. [CrossRef]
11. Chamara, N.; Islam, M.D.; Bai, G.; Shi, Y.; Ge, Y. Ag-IoT for Crop and Environment Monitoring: Past, Present, and Future. *Agric. Syst.* **2022**, *203*, 103497. [CrossRef]
12. Ma, D.; Maki, H.; Neeno, S.; Zhang, L.; Wang, L.; Jin, J. Application of Non-Linear Partial Least Squares Analysis on Prediction of Biomass of Maize Plants Using Hyperspectral Images. *Biosyst. Eng.* **2020**, *200*, 40–54. [CrossRef]
13. Adão, T.; Hruška, J.; Pádua, L.; Bessa, J.; Peres, E.; Morais, R.; Sousa, J.J. Hyperspectral Imaging: A Review on UAV-Based Sensors, Data Processing and Applications for Agriculture and Forestry. *Remote Sens.* **2017**, *9*, 1110. [CrossRef]
14. Deng, L.; Mao, Z.; Li, X.; Hu, Z.; Duan, F.; Yan, Y. UAV-Based Multispectral Remote Sensing for Precision Agriculture: A Comparison between Different Cameras. *ISPRS J. Photogramm. Remote Sens.* **2018**, *146*, 124–136. [CrossRef]
15. Olson, D.; Anderson, J. Review on Unmanned Aerial Vehicles, Remote Sensors, Imagery Processing, and Their Applications in Agriculture. *Agron. J.* **2021**, *113*, 971–992. [CrossRef]
16. Wang, L.; Chen, S.; Li, D.; Wang, C.; Jiang, H.; Zheng, Q.; Peng, Z. Estimation of Paddy Rice Nitrogen Content and Accumulation Both at Leaf and Plant Levels from UAV Hyperspectral Imagery. *Remote Sens.* **2021**, *13*, 2956. [CrossRef]
17. Liu, Y.; Feng, H.; Yue, J.; Fan, Y.; Jin, X.; Zhao, Y.; Song, X.; Long, H.; Yang, G. Estimation of Potato Above-Ground Biomass Using UAV-Based Hyperspectral Images and Machine-Learning Regression. *Remote Sens.* **2022**, *14*, 5449. [CrossRef]
18. Côté, P.-O.; Nikanjam, A.; Ahmed, N.; Humeniuk, D.; Khomh, F. Data Cleaning and Machine Learning: A Systematic Literature Review. *Autom. Softw. Eng.* **2024**, *31*, 54. [CrossRef]
19. Pereira, L.G.; Fernandez, P.; Mourato, S.; Matos, J.; Mayer, C.; Marques, F. Quality Control of Outsourced LiDAR Data Acquired with a UAV: A Case Study. *Remote Sens.* **2021**, *13*, 419. [CrossRef]
20. Hsiao, C.-H.; Lai, Y.-H.; Kuo, S.-Y.; Cai, Y.-H.; Lin, C.-H.; Wang, Y.-S. A Dynamic Data Correction Method for Enhancing Resolving Power of Integrated Spectra in Spectroscopic Analysis. *Anal. Chem.* **2020**, *92*, 12763–12768. [CrossRef]
21. Silalahi, D.D.; Midi, H.; Arasan, J.; Mustafa, M.S.; Caliman, J.-P. Robust Generalized Multiplicative Scatter Correction Algorithm on Pretreatment of near Infrared Spectral Data. *Vib. Spectrosc.* **2018**, *97*, 55–65. [CrossRef]
22. Vašát, R.; Kodešová, R.; Klement, A.; Borůvka, L. Simple but Efficient Signal Pre-Processing in Soil Organic Carbon Spectroscopic Estimation. *Geoderma* **2017**, *298*, 46–53. [CrossRef]
23. Long, S.P.; Zhu, X.; Naidu, S.L.; Ort, D.R. Can Improvement in Photosynthesis Increase Crop Yields? *Plant Cell Environ.* **2006**, *29*, 315–330. [CrossRef] [PubMed]
24. Katz, J.J.; Norris, J.R. Chlorophyll and Light Energy Transduction in Photosynthesis. Work Performed under the Auspices of the U.S. Atomic Energy Commission. In *Current Topics in Bioenergetics*; Elsevier: Amsterdam, The Netherlands, 1973; Volume 5, pp. 41–75. ISBN 978-0-12-152505-7.
25. Atta, B.M.; Saleem, M.; Ali, H.; Arshad, H.M.I.; Ahmed, M. Chlorophyll as a Biomarker for Early Disease Diagnosis. *Laser Phys.* **2018**, *28*, 065607. [CrossRef]
26. Leghari, S.J.; Wahocho, N.A.; Laghari, G.M.; HafeezLaghari, A.; MustafaBhabhan, G.; HussainTalpur, K.; Bhutto, T.A.; Wahocho, S.A.; Lashari, A.A. Role of Nitrogen for Plant Growth and Development: A Review. *Adv. Environ. Biol.* **2016**, *10*, 209–219.
27. Haralick, R.M.; Shanmugam, K.; Dinstein, I. Textural Features for Image Classification. *IEEE Trans. Syst. Man Cybern.* **1973**, *SMC-3*, 610–621. [CrossRef]
28. Liang, W.; Haiyan, C.; Jiangpeng, Z.; Jiafei, Z.; Xiaoyue, D.; Yong, H. Using Fusion of Texture Features and Vegetation Indices from Water Concentration in Rice Crop to UAV Remote Sensing Monitor. *Smart Agric.* **2020**, *2*, 58. [CrossRef]
29. Zahir, S.A.D.M.; Jamlos, M.F.; Omar, A.F.; Jamlos, M.A.; Mamat, R.; Muncan, J.; Tsenkova, R. Review—Plant Nutritional Status Analysis Employing the Visible and near-Infrared Spectroscopy Spectral Sensor. *Spectrochim. Acta. A Mol. Biomol. Spectrosc.* **2024**, *304*, 123273. [CrossRef]
30. Sun, K.; Geng, X.; Ji, L.; Lu, Y. A New Band Selection Method for Hyperspectral Image Based on Data Quality. *IEEE J. Sel. Top. Appl. Earth Obs. Remote Sens.* **2014**, *7*, 2697–2703. [CrossRef]
31. Zhao, H.; Wang, Z.; Jia, G.; Tian, J.; Jin, S.; Liang, S.; Liu, Y. The Impact and Correction of Sensitive Environmental Factors on Spectral Reflectance Measured In Situ. *Remote Sens.* **2023**, *15*, 5332. [CrossRef]
32. Shu, M.; Zuo, J.; Shen, M.; Yin, P.; Wang, M.; Yang, X.; Tang, J.; Li, B.; Ma, Y. Improving the Estimation Accuracy of SPAD Values for Maize Leaves by Removing UAV Hyperspectral Image Backgrounds. *Int. J. Remote Sens.* **2021**, *42*, 5862–5881. [CrossRef]

33. Sudu, B.; Rong, G.; Guga, S.; Li, K.; Zhi, F.; Guo, Y.; Zhang, J.; Bao, Y. Retrieving SPAD Values of Summer Maize Using UAV Hyperspectral Data Based on Multiple Machine Learning Algorithm. *Remote Sens.* **2022**, *14*, 5407. [CrossRef]
34. Meiyan, S.; Jinyu, Z.; Xiaohong, Y.; Xiaohe, G.; Baoguo, L.; Yuntao, M. A Spectral Decomposition Method for Estimating the Leaf Nitrogen Status of Maize by UAV-Based Hyperspectral Imaging. *Comput. Electron. Agric.* **2023**, *212*, 108100. [CrossRef]
35. Osco, L.P.; Junior, J.M.; Ramos, A.P.M.; Furuya, D.E.G.; Santana, D.C.; Teodoro, L.P.R.; Gonçalves, W.N.; Baio, F.H.R.; Pistori, H.; Junior, C.A.D.S.; et al. Leaf Nitrogen Concentration and Plant Height Prediction for Maize Using UAV-Based Multispectral Imagery and Machine Learning Techniques. *Remote Sens.* **2020**, *12*, 3237. [CrossRef]